Geodesy and Geodynamics 8 (2017) 433–442

Contents lists available at ScienceDirect

Geodesy and Geodynamics

journal homepages: www.keaipublishing.com/en/journals/geog;
http://www.jgg09.com/jweb_ddcl_en/EN/volumn/home.shtml

Multichannel singular spectrum analysis of the axial atmospheric angular momentum

Leonid Zotov [a, *], N.S. Sidorenkov [b], Ch. Bizouard [c], C.K. Shum [d, e], Wenbin Shen [f]

[a] National Research University Higher School of Economics, Moscow Institute of Electronics and Mathematics, Russia
[b] Hydro-Meteorological Center of Russia, Global Atmospheric Circulation Laboratory, Russia
[c] SYRTE, Observatoire de Paris, PSL Research University, CNRS, Sorbonne Universit es, UPMC Univ., Paris 06, France
[d] Division of Geodetic Science, School of Earth Sciences, The Ohio State University, USA
[e] Institute of Geodesy & Geophysics, Chinese Academy of Sciences, Wuhan, China
[f] Department of Geophysics, School of Geodesy and Geomatics, Key Laboratory of Geospace Environment and Geodesy of Ministry of education, Wuhan University, Wuhan 430079, China

ARTICLE INFO

Article history:
Received 16 November 2016
Accepted 20 February 2017
Available online 16 June 2017

Keywords:
Earth's variable rotation
Atmospheric circulation
AAM (Atmospheric angular momentum)
MSSA (Multichannel singular spectrum analysis)
ENSO (El Nino southern oscillation)
LOD (Length of day)

ABSTRACT

Earth's variable rotation is mainly produced by the variability of the AAM (atmospheric angular momentum). In particular, the axial AAM component χ_3, which undergoes especially strong variations, induces changes in the Earth's rotation rate. In this study we analysed maps of regional input into the effective axial AAM from 1948 through 2011 from NCEP/NCAR reanalysis. Global zonal circulation patterns related to the LOD (length of day) were described. We applied MSSA (Multichannel Singular Spectrum Analysis) jointly to the mass and motion components of AAM, which allowed us to extract annual, semiannual, 4-month, quasi-biennial, 5-year, and low-frequency oscillations. PCs (Principal components) strongly related to ENSO (El Nino southern oscillation) were released. They can be used to study ENSO-induced changes in pressure and wind fields and their coupling to LOD. The PCs describing the trends have captured slow atmospheric circulation changes possibly related to climate variability.

1. Introduction

Exchange of angular momentum between the atmosphere, the ocean, and the solid Earth was found to be the main cause of Earth's variable rotation, composing of the LOD (length of day) variations and polar motion. The atmospheric influence on the Earth's rotation rate is especially large due to the fact that the atmosphere having much larger mobility than the ocean, tends to be in zonal flow direction without closed gyres. The axial (along the parallels, orthogonal to the rotation axis) component of the angular momentum changes, related to zonal circulation, is the largest one (approximately 5×10^{25} kg·m^2/s) [1,2]. Thus, its study is of crucial importance for understanding the causes of the variable rotation of the Earth and of the atmosphere. In this work we treat only axial AAM (atmospheric angular momentum) component.

AAM can be calculated based on the meteorological data and NWP (numerical weather prediction) models from different meteorological centers, such as NCEP/NCAR, JMA, and ECMWF [3]. AAM integrated over the globe and converted to ms units is called EAAM (effective atmospheric angular momentum). It can be used to study LOD changes and their causes, after zonal tides (according to Ref. [4]) and some other effects have been removed. Such studies were reported by numerous authors [5–10], and it has been shown that the atmosphere induces major excitations with wide ranges of frequency bands – from days to years – into the LOD changes.

To demonstrate this, we plotted the axial global EAAM and LOD variations in Fig. 1a. We separated the high-frequency and low-frequency oscillations of LOD, after the zonal tides were removed according to IERS convention model, using a filter as shown by Eq. (4) with the cut-off frequency f_0=1/500 days^{-1}. It is seen that high-

* Corresponding author. National Research University Higher School of Economics, Moscow Institute of Electronics and Mathematics, Russia.
E-mail address: wolftempus@gmail.com (L. Zotov).
Peer review under responsibility of Institute of Seismology, China Earthquake Administration.

Production and Hosting by Elsevier on behalf of KeAi

http://dx.doi.org/10.1016/j.geog.2017.02.010

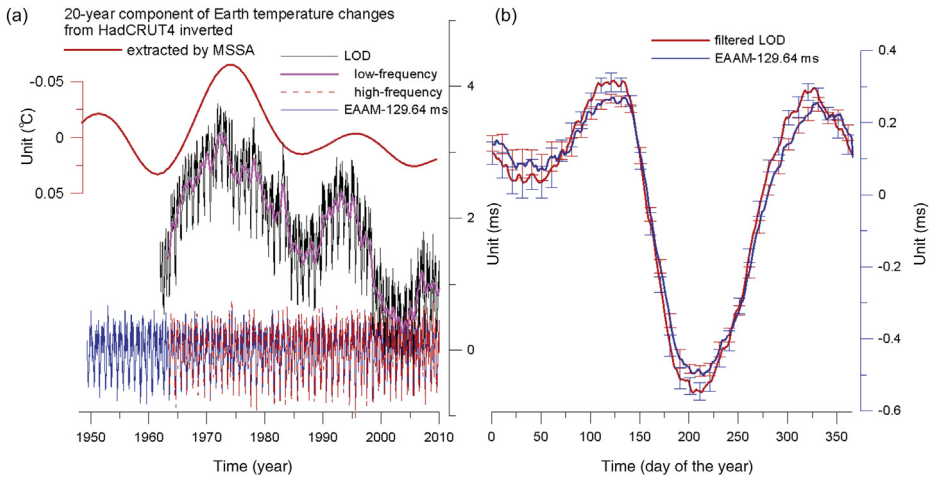

Fig. 1. (a) High- and low-frequency LOD changes, EAAM (wind + IB-pressure) variability and 20-year global temperature mode. (b) EAAM and LOD changes, averaged over the days of the year on 1962–2010 interval.

frequency LOD variations correspond very well to EAAM (wind + IB-pressure) changes. Correlation coefficient for the period 1962–2010 is 0.959±0.001. High-frequency EAAM and LOD variations averaged for each day of the year are shown in Fig. 1b. Correlation between the quantities is 0.992±0.002. This leaves no doubt in the axial momentum exchange between the atmosphere and the solid Earth, there is almost no ocean buffering at these frequencies.

With regard to low-frequency (decadal or longer) variations of the LOD, they can not be explained solely by the atmospheric processes and require input from the ocean and the core [11]. We found out that the 60- and 20-year component of the Global Mean Earth Temperature changes (HadCRUT4) extracted using the MSSA (Multichannel Singular Spectrum Analysis) [12,13], are anti-correlated with the low-frequency changes in LOD (Fig. 1a. To find the reasons, one needs to study different modes of zonal atmospheric circulation, for their possible correlations with natural and anthropogenic climate change signals geographically. In this work we employed an innovative technique, the MSSA, to improve the decompositions of the AAM maps into various PCs (principle components).

Influence of atmosphere on the Earth rotation can be decomposed into the influence of winds and pressures. Thus, the axial EAAM χ_3 includes two components: pressure (mass) χ_3^P and wind (motion) χ_3^W. The first one is related to the changes of atmospheric tensor of inertia, the second one is related to the relative angular momentum of zonal winds. The Earth is decelerated when the atmospheric moment of inertia χ_3^P increases, resulting from the redistribution of the air mass. According to the conservation of momentum principle, the increase of χ_3^W also leads to the deceleration of the Earth's rotation rate and LOD increase. Westerly winds, taking the momentum out from the solid Earth, produce positive input into the EAAM, at the same time decelerating Earth rotation. Increase of easterly winds, vise versa, accelerates the Earth and decelerates the atmospheric superrotation. On average, in 70 days atmosphere makes 71 rotations around the Earth axis [14]. The latter is seen from the positive mean value of the wind EAAM term. Its mean value is $<\chi_3^W> = 1.4 \times 10^{26}$ kg·m^2/s, and its standard deviation is $\sigma_{\chi_3^W} = 2.3 \times 10^{25}$ kg·m^2/s. Pressure term (IB) mean is $<\chi_3^P> = 102 \times 10^{26}$ kg·m^2/s, and its standard deviation is $\sigma_{\chi_3^P} = 0.4 \times 10^{25}$ kg·m^2/s. Converted to milliseconds in LOD, these values correspond to $<\chi_3^W> = 2.34$ ms, $\sigma_{\chi_3^W} = 0.384$ ms, $<\chi_3^P> = 127.29$ ms, $\sigma_{\chi_3^P} = 0.055$ ms. Wind variability is larger than the pressure variations, but the latter has a larger mean. Fig. 1b shows that maxima in EAAM occur in May (1/05) and December (7/12), minima – in August (4/08) and February (27/02), and they are mainly determined by seasonal wind changes.

The goal of this work was to study the axial AAM components represented in the form of maps (multidimensional time series) by means of MSSA (Multichannel Singular Spectrum Analysis), to detect physical signals in AAM and LOD through it. Being a generalization of the Empirical Orthogonal Functions (EOF) method, well known in atmospheric and climate research [15–18], MSSA is more flexible than simple EOF by allowing one to more effectively separate different frequencies and filter out noises of multidimensional data [19].

Similar study of the axial AAM over the interval 1970–1998 was earlier performed [20–22]. In the last two papers AAM averages in 20 longitude belts were processed by MSSA. MSSA was also applied to 1104 spatial sector elements of AAM maps by Ref. [23]. El Nino pattern was revealed in the 5- and 2-year frequency bands, illustrating its propagation to the polar regions in the latitude-time Hovmoeller plots. Our work extends the previous studies to the regional values of AAM being given on the latitude–longitude grid and with a longer time span (1948–2010). For the first time the joint MSSA for mass and motion AAM terms was performed. This technique based on joining two components into complex lagged trajectory matrix revealed coupled changes in both terms and allowed enhanced principal component decompositions. Animated maps obtained allow to quantify the behavior of different components, including their relationship to, but not limited to El Nino. The components were not obtained with pre-designed filters, but directly computed from MSSA.

The mathematical basis of our study will be provided in the next section. The initial data and method of their conversion will also be described. You may find MSSA method in the third section and the results in the fourth section. In conclusion the applicability of results to the Earth's rotation studies and the perspectives of the method will be discussed.

2. Model equations and data

The Euler–Liouville equation of the rotating Earth [24,25] states for the small correction m_3 to the Earth's angular velocity $\Omega(1 + m_3)$:

$$m_3 = \psi_3 \tag{1}$$

Here the axial component of excitation ψ_3 stands to the right. It can be considered as input, producing changes of Earth's rotation rate m_3. The excitation depends on variations of the Earth's inertia tensor, resulting from the redistribution of mass, relative movement of matter (winds and currents), and external forces. Processes in atmosphere, ocean, Earth's core, and mantle influence planetary rotation, providing the corresponding excitation. Below we restrict our consideration only to the axial atmospheric excitation.

In the Euler–Liouville equation (1) the variable m_3 can be expressed through LOD changes as $m_3 = -\Delta LOD/LOD$ [26,27]. Instead of excitation function it is better to use the EAAM (effective angular momentum) function χ, whose axial component differs only in sign, $\psi_3 = -\chi_3$. Good agreement between LOD variability and global EAAM, as seen from Fig. 1, allows us to assume in this work that $\Delta LOD/LOD = \chi_3$ holds, and all the components of χ_3 obtained below influence Earth's rotation, resulting in LOD variations. To have a suitable unit to estimate this effect throughout this article we will multiply χ_3 by the conventional value of LOD = 86,400,000 ms, converting EAAM units to milliseconds. In contrast to global EAAM, we call the regional inputs as AAM (without E).

We used NCEP/NCAR reanalysis data which were obtained through meteorological data processing with use of NWP (numerical weather prediction). The interpolated fields of wind and pressure all over the globe are available since 1948 with 6-hour steps. The data for different heights (pressure levels) can be found at http://www.esrl.noaa.gov/psd/data/gridded/data.ncep.reanalysis.html.

These data were processed and converted to AAM maps at the Center for Astro-geodynamics of Shanghai Astronomical Observatory (Y.H. Zhou, personal communication). At every geographical data point the pressure component was calculated according to the expression

$$X_3^P(\lambda,\phi) = \frac{0.756R^4}{C_m g} p_s(\lambda,\phi)\cos^3\phi \tag{2}$$

and the wind component – according to

$$X_3^W(\lambda,\phi) = \frac{R^3}{C_m \Omega g}\int u(\lambda,\phi,p)\cos^2\phi \mathrm{d}p \tag{3}$$

where R and Ω are mean Earth's radius and angular velocity, C_m is the principal moment of inertia of the mantle around Earth's rotation axis, g is the gravitational acceleration, λ and ϕ are longitude and latitude of a grid point, p is pressure level, p_s is surface pressure, u is zonal wind velocity and is integrated for the selected grid cell. The pressure component reduced to the surface was calculated, according to Eq. (2), taking into account the IB ("inverted barometer") hypothesis [28]. Eq. (3) requires integration along the atmospheric pressure levels. Thus, not only the surface winds but also winds in troposphere and stratosphere account for this term [29].

As a result, the maps of effective AAM with 6-hour temporal steps and 2.5° × 2.5° angular resolution were obtained. The processing of 50 years of data at fine spatial resolution requires intensive computer resources. Our resources were limited (AMD with 4 cores, 32 Gb of memory) and the grid was converted to 5° × 5° resolution containing 35 × 72 = 2520 points (poles excluded) by summation in the corresponding regions. Before applying MSSA, we also reduced the temporal resolution. The time series for every cell was filtered with the Panteleev low frequency filter, whose impulse response is

$$h(t) = \frac{\omega_0}{2\sqrt{2}} e^{-\frac{\omega_0|t|}{\sqrt{2}}}\left(\cos\frac{\omega_0 t}{\sqrt{2}} + \sin\frac{\omega_0|t|}{\sqrt{2}}\right) \tag{4}$$

with parameter $\omega_0 = 2\pi f_0$, defining the cut-off frequency [30]. The parameter value $f_0 = 10\ \mathrm{yr}^{-1}$ was selected. Then the data were resampled by decimation with 10-day steps without any distortion of filtered low-frequency component. Such preprocessing reduced the data volume by 4 times through spatial resampling, then by 40 times through temporal resampling.

Integration (summation) over all the longitudes and latitudes gives EAAM

$$\chi_3^{P,W} = \int\int X_3^{P,W}(\lambda,\phi)\mathrm{d}\lambda\mathrm{d}\phi \tag{5}$$

EAAM check showed that it completely coincides with data (not gridded) provided by IERS (http://www.iers.org/IERS/EN/DataProducts/GeophysicalFluidsData/geoFluids.html).

Global EAAM after Panteleev's filtering is shown as initial data by the black line in Fig. 2: (a) is shown for pressure, while (c) is for wind component. Their spectrograms are shown by thick lines in Fig. 3. The peaks with periods 1, 1/2, and 1/3 of a year can be clearly identified.

3. Multichannel singular spectrum analysis

Multichannel Singular Spectrum Analysis (MSSA), also called Extended EOF, is a generalization of Singular Spectrum Analysis (SSA) for multidimensional (multichannel) time series [31,32]. SSA in its turn is the Principal Component Analysis generalized for time series, so that the trajectory matrix, rather than simple correlation matrix, is analyzed. It is obtained by means of time series embedding into the L-dimensional space.

At every point of the map we have a time series (channel), which could be studied through SSA. The main parameter of the method is a lag L. The time series segments of L points are to be put sequentially as columns into the trajectory matrix, then are subject to the Singular Value Decomposition (SVD). As a result, a sequence of singular numbers (SNs) in order of decreasing values and corresponding eigenvectors are obtained. The principal components (PCs) can be reconstructed from them. It may well be that some of SNs are related to the same PC. In this instance the corresponding SN-components have to be grouped together and reconstructed as one PC. The grouping methods given in Ref. [33] are based on recognition of SN-components having similar behavior. Finally, the set of PCs with decreasing amplitudes representing different modes of time series variability is obtained. The method allows one to extract periodic components with changing amplitudes, to separate the trend, noise, etc. The details of the method can be found in the works [30,32–35].

The main difference between MSSA and SSA is that in MSSA the trajectory matrices for every time series (every pixel of an image) are joined into one block trajectory matrix. In our MSSA realization we put the trajectory matrices for every channel one under another, which up to transposition coincides with the standard technique described in Ref. [32].

In this study we applied joint MSSA to mass and motion terms, when they are incorporated into large block trajectory matrix together. Most of the PCs require SNs pairs grouping. As a result, the PC's maps can be obtained, representing the main components of variability of the geophysical fields in this study. Such maps demonstrate spatio-temporal regions with correlated behavior more evidently.

There are several recommendations for parameter L selection [36]. It has to be less than half of the time series length, preferably,

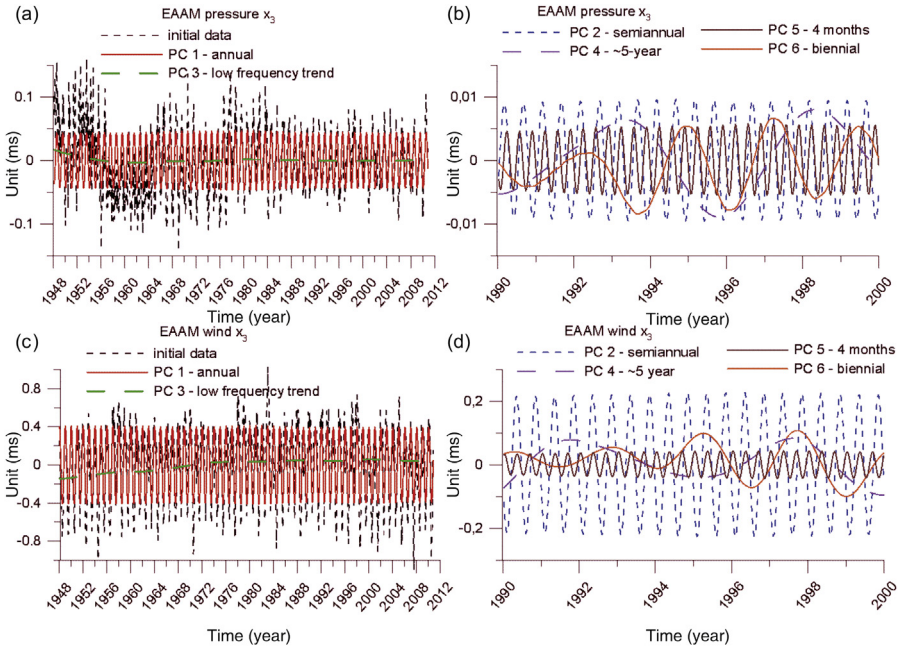

Fig. 2. AAM principal components (PCs) for pressure (a and b) and wind (c and d) terms integrated all over the globe. Annual PC 1 and low-frequency trend PC 3 compared to the initial data on the (a) and (c). Plots on the (b) and (d) are given from 1990 to 2000 yr. They represent the PC 2,4,5,6 related to the semiannual, quasi-5-year, 4-monthly, and quasi-biennial oscillations, respectively.

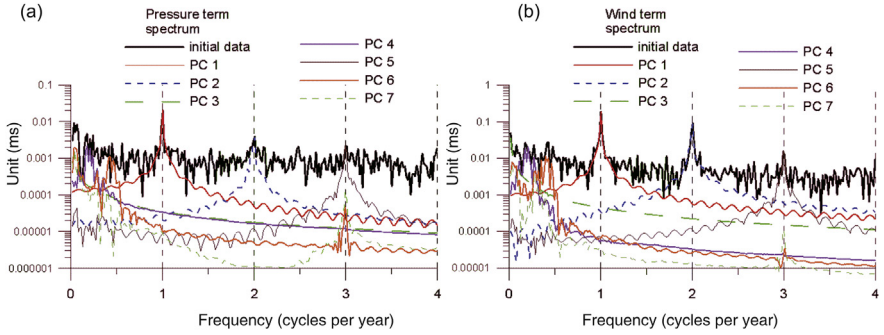

Fig. 3. Integrated PCs spectra for pressure (a) and wind (b). Thick solid curves give spectra of initial data. Other curves give spectra of PCs. PC 1 has annual periodicity, PC 2 – semiannual, PC 3 corresponds to the low-frequency trend, PC 4 – to 5-yr ENSO pattern, PC 5 has period of 4 months, PC 6 and PC 7 are related to the quasi-biennial and low-frequency oscillation teleconnected to ENSO.

being the multiples of periods of the expected oscillations. Strict result on asymptotic stability states, that within such a strategy the separability of mutually orthogonal components is improving with increase of the time series length. L selection strategy is heuristic and the results for different L values have to be compared. From spectrum analysis in Fig. 3, we expect the presence of components whose periods are multiples of a year. We performed comparisons for L being equal to 2, 5, 6, and 18 years, finding the results more or less similar. With increase of L the trajectory matrix size grows, and its processing becomes more consuming, at the same time the extraction of the low-frequency PCs improves. Relatively good quality of separation was achieved for L being equal to 6 years ($L = 219$ for maps with 10-day step), which was finally selected.

To compare the results with simple EOF, we performed calculations for the case of $L = 1$ (no lag), when simple correlation matrix is analyzed without signal embedding into the multidimensional space. It turned out that simple EOF only allows one to separate the annual component as the first PC, with all other components representing the sequence of noisy mixed signals of increasing frequency and decreasing amplitude. Earlier it has already been shown [34,37,38] that simple EOF has limited potential to separate the trend from annual and semiannual components, and is less effective than MSSA to operate on variable geophysical fields. The tests presented in cited papers have also shown that MSSA recovers more than 90% of variability of the simulated annual, semiannual and long-periodic signals mixed with noises.

Separate MSSA application to mass and motion terms was also tested. The reconstructed PCs were very similar to that obtained by joint MSSA, with only small variations in amplitude and different sequence of singular numbers to be grouped. It means that the PCs obtained are really the main stable modes of AAM pressure and wind changes. On the other hand, joint processing improved the signals separation uncovering the couple effects.

4. Joint MSSA of AAM mass and motion terms

Before MSSA processing, average wind and pressure fields over the 62-year interval were subtracted.[1] Their maps are presented in

[1] Without subtracting before MSSA, the mean will be reconstructed as the first PC.

Fig. 4 together with plots obtained by integration over meridians and parallels. The average maps represent the constant part of the zonal circulation and pressure distribution.

Pressure mean, Fig. 4a. The largest pressure input into EAAM comes from the equatorial belt, emphasizing its part over the ocean, quickly decreasing at ±30° latitudes. Generally, the mass term gives larger mean input into EAAM than the motion term. Input from the mountain and polar regions is smaller, which can be well seen in the plots which were obtained through integration over meridians and pictured above and below the maps in Fig. 4.

Wind mean, Fig. 4b. The wind minima are along the equator and maxima are along the ±45° latitudes. The wind minima (negative extrema) along the equator is due to strong easterly winds blowing in stratosphere at low latitudes. The change of the zonal winds occurs in the so-called "horse latitudes" at ±30° in both hemispheres. The latitudes from 30° to 60° and −30° to −60° can be characterized by large westerly winds and tropospheric currents. Westerly winds prevail in the atmosphere, containing an excess of angular momentum (atmosphere rotates slightly quicker than the rigid Earth). According to the zonal circulation theory [2,39,40], the angular momentum is pumped into atmosphere at low latitudes

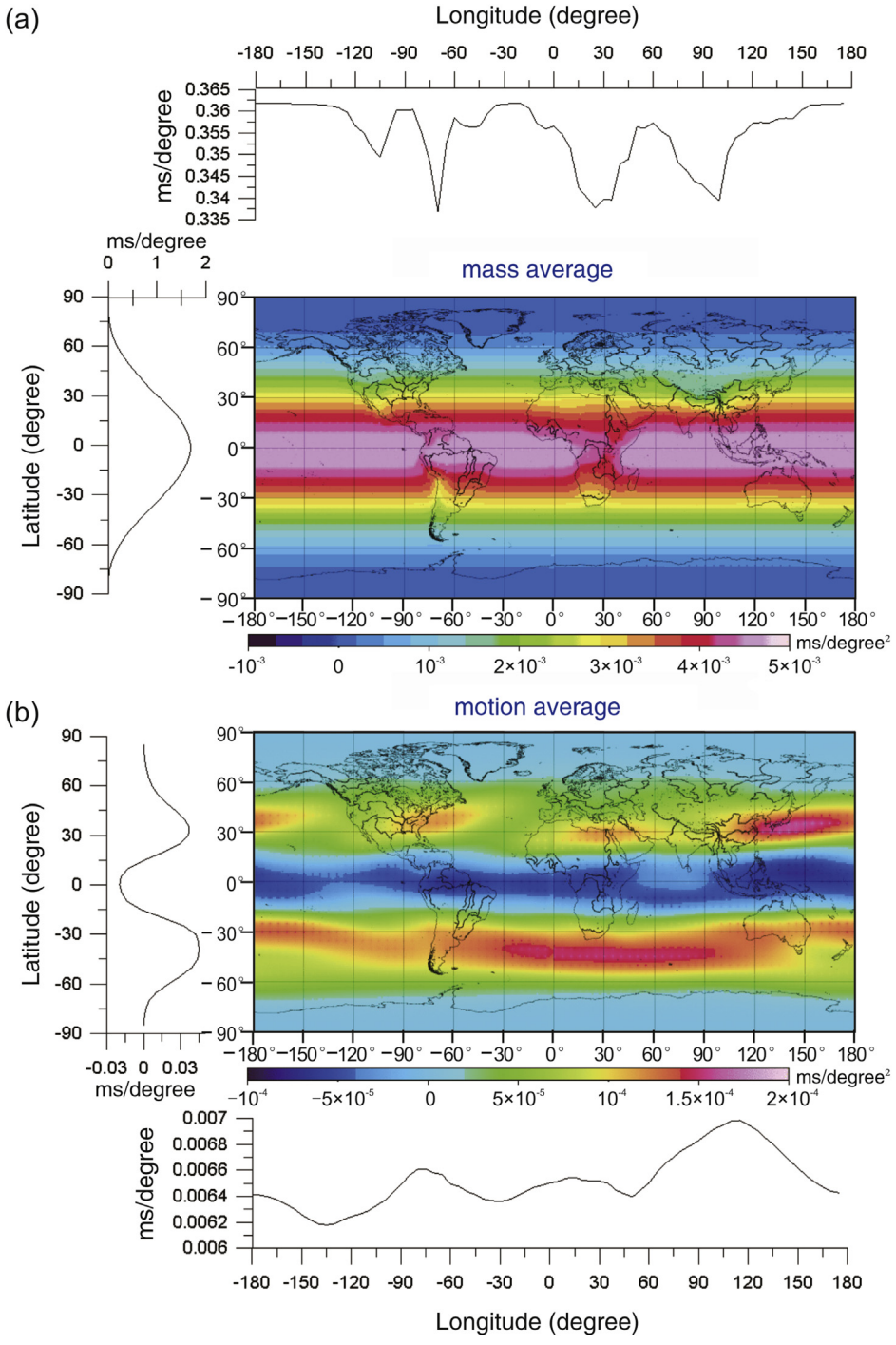

Fig. 4. Mean (average) pressure (a) and wind (b) terms. Plots to the (a) and (b) and to the left of the maps represent the sum over meridians and parallels in 5° belts.

and returns to the rigid Earth in the zone of westerly winds (350°–60° N and S latitudes).

After average subtraction we performed MSSA processing jointly for mass and motion terms. It helps to obtain the PCs of axial AAM variability, representing coupled changes in both terms. The corresponding maps were animated and placed as Supplemental materials at http://lnfm1.sai.msu.ru/~tempus/science/MSSA/ATMZ/.

EAAM curves for the PCs calculated through integration over the globe are shown in Fig. 2: (a) and (b) for the pressure components, (c) and (d) for the wind components. Fig. 3 represents the spectra of integrated PCs in order to demonstrate which frequencies the PCs correspond to. Every PC gives a portion of the signal spectrum, with the sum of all PCs reconstructing the exact initial signal. The plots in Figs. 2 and 3 prove that MSSA of the wind and pressure terms allowed us to extract long-periodic trend and oscillations with periods 5, 2, 1, 1/2, 1/3 of a year. In Table 1 standard deviations are given for the first seven PCs of wind and pressure terms. They absorb most of the signal variability (power) and below we will describe them in detail. The components with higher numbers (SN > 12) have smaller amplitudes and include mostly noises. They look like random high-frequency variations on the maps, their analysis is not attempted in this study.

PC 1 of pressure (obtained by grouping of 1 and 2 SN) reflects the annual cycle of pressure change. The changes over the continents are much larger than that over the ocean, which is easy to explain as a result of pressure compensation by water level changes over the sea, accounting for the inverted barometer effect. In January the positive input comes from the northern hemisphere, and the negative is from the southern hemisphere. It is related to the anticyclonic circulation, air mass increase in winter hemisphere, and its redistribution to the continents.

The beginning of the year can be characterized by overall integrated minimum of PC 1 (Fig. 2a), with the regions accelerating the Earth (AAM minima) prevailing over the decelerating regions (AAM maxima). Negative input is located over South America, Africa to the south from equator, Tibet, and especially Australia. Positive input is observed over Arabian peninsula, India, and Eastern China. Less strong positive input comes from the Sahara, South of Aral, North coast of the Gulf of Mexico. By the end of June the picture inverts: the geographical regions with the AAM maxima become the minima, while the minima become the maxima. Generally, the air mass in the northern/southern hemispheres increases in the winter, and decreases in the summer. The pressure over the ocean, being equilibrated by "inverted barometer", is smaller in January than that in July, which can be explained by air mass redistribution from the ocean to the continents. The observations of the opposite PC 1 contribution in the mountains (Tibetan Plateau) and nearby valleys agree well with results obtained by Ref. [2].

PC 1 of wind (1 + 2 SN) reflects annual oscillation having integrated maximum at the beginning of the year in opposite phase to the pressure PC 1. The amplitude of the wind component is one order of magnitude higher than the pressure one (Table 1), thus it defines the overall AAM variability and the annual maxima and minima of LOD (Fig. 1b). The influence of the wind component over the ocean is slightly larger than that over the continents, with regions of the same sign being elongated along the parallels with small inclination to the North-East.

Table 1
The standard deviations (STD) of PCs in ms. The amplitude of sin wave is approximately $\sqrt{2}$ of its STD.

	All	PC 1	PC 2	PC 3	PC 4	PC 5	PC 6	PC 7
mass $\times 10^{-2}$	4.84	3.14	0.73	0.34	0.54	0.42	0.57	0.28
motion $\times 10^{-1}$	3.77	2.84	1.60	0.61	0.53	0.30	0.39	0.17

The state especially contrasts at the end of January, with maximum stripe stretching around 30° (slightly inclined) north parallel and stripe of less intensive minimum banding all over the Earth at 30° south. The picture changes to the opposite by the end of July. At this time the minimum is visible in wind AAM and LOD variations, which means acceleration of the Earth's rotation.

PC 2 of pressure (3 + 4 SN) represents the semiannual oscillation. The extrema of this component were found to have a one month delay with respect to the extrema and zeros of annual PC 1. In January and July, PC 2 has maxima over Africa, emphasizing the South of Sahara, Brazil, Mexico, and South of US, minima over Eastern Canada, Australia, and almost all of Asia. Integrated PC 2 of pressure component has maxima in these months. The picture inverts in April and October.

PC 2 of wind (3 + 4 SN) is semiannual with integrated minima at the beginning and middle of the year, coinciding with extrema of the annual oscillation. The pattern of PC 2 is quite complicated. The zone of maximum at the 25° north over the Pacific ocean is accompanied by minima over the Atlantic ocean, West Sahara, Mexico, North and Equatorial Pacific, Indian Ocean to the West from Australia. The picture inverts with half period of 3 months.

According to Ref. [2], the annual and semiannual components of relative momentum change physically follow from the same process – the work of hemispherical heat engine transferring the air mass from one hemisphere to another and changing zonal circulation type of the relocated air mass. As a result of overheating of the northern hemisphere with respect to the southern hemisphere, χ_3^W has deep minimum in August and less deep minimum in February (Fig. 1b). This joint effect is represented as annual and semiannual oscillations in MSSA decomposition.

PC 3 of pressure (5 SN) reflects slow changes (trend). The difference between 1948 and 2011 is shown in Fig. 5. During this period the atmospheric mass increases over South America, Africa, Western Europe, Asia and Australia. The pattern is especially intensive in Sahara desert. The increase of pressure AAM over the continents is accompanied by its decrease over the ocean. Fig. 5c shows integrated decrease for this PC.

PC 3 of wind (5 SN) representing the trend is shown in Fig. 5. The difference between 1948 and 2011 shows AAM increase around equator and 60° south, accompanied by the decrease at 30° south. It could be attributed to the increase of the westerly winds over equator and Antarctic circumpolar circulation region, and easterly winds component increase at 30° south. The total increase of EAAM for this PC is seen from Fig. 5d. Low-frequency changes of climatological origin including the trend in ENSO intensity can be attributed to PC 3.

Fig. 5 for PC 3 shows that AAM pressure term decreases over the continents and increases over the ocean. It accelerates the Earth by approximately 0.02 ms in 60 years. But this effect is overlapped by the dominant wind AAM decrease, caused by the westerlies intensification, which, due the conservation principal, decelerates the Earth by approximately 0.25 ms in 60 years, causing LOD increase. These results qualitatively agree with the results of Ref. [5], whose estimates of the effects in LOD under the sceptical Global Warming scenarios for 60 years in the future are: −0.05 ms for AAM mass term, and 0.11 ms for wind effect. The proposed reasons were: the polar shift of atmospheric pressure, causing the change of the atmosphere flattening and acceleration of the Earth from one side; zonal winds increase, especially in the southern hemisphere, causing dominant slow-down effect from another side. That is similar to which is observed for PC 3 in Fig. 5. Still we cannot exclude the influence of AAM noise and artefacts on this PC. For example, the increase of number of meteorological stations since 1950 could affect the accuracy of the estimated trend (see https://esrl.noaa.gov/psd/cgi-bin/data/ISPD/stationplot.v2.pl).

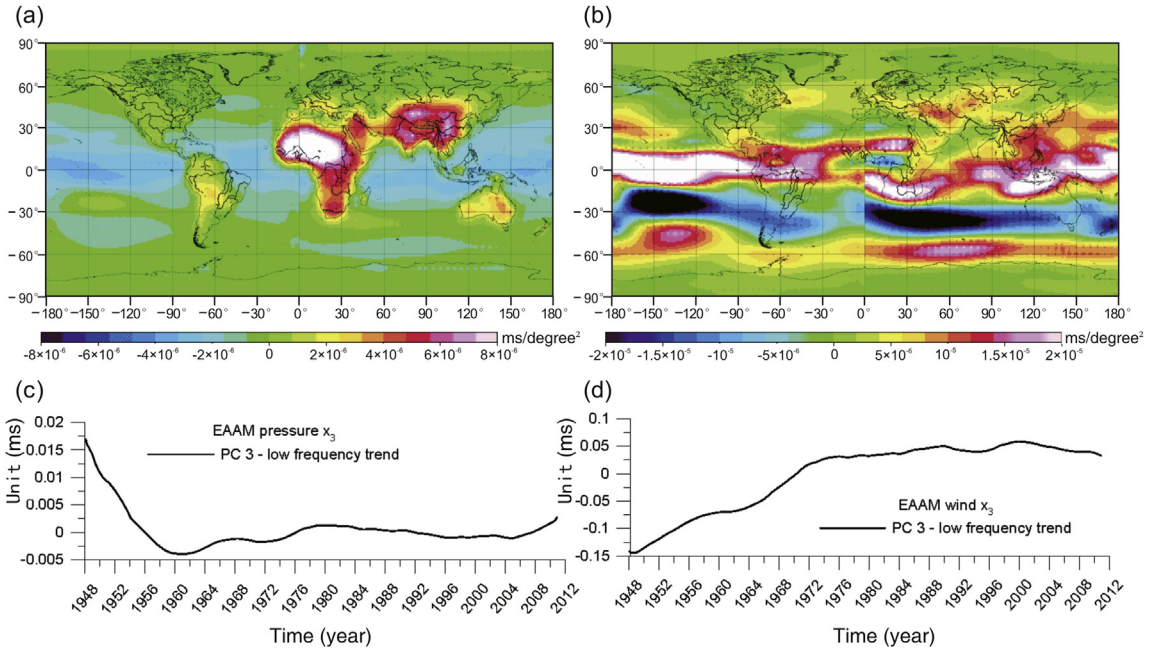

Fig. 5. The maps of difference between 1948 and 2011 for PC 3 atmospheric pressure (a and c) and wind (b and d) term and the corresponding plots of integrated EAAM below.

PC 4 (6 + 7 SN) has period of approximately 5 years for both terms. The three maps of PCs 4 are presented in Fig. 6 a,c,e for pressure and b,d,f for wind. The strongest pressure changes are over the continents surrounding the Indian ocean, while the wind changes are mostly pronounced in the Eastern Pacific. We compared the integrated PC 4 to the Southern Oscillation Index (SOI) describing the activity of ENSO. SOI curve was preliminary inverted and smoothed by the Panteleev filter (4) with parameter $f_0 = 0.3$ yrs^{-1}. Comparison presented in Fig. 7 indicates that PC 4 is related to ENSO. The maxima and minima of pressure and wind terms correspond well to each other and to SOI extrema. The correlation coefficient is $r = -0.72 \pm 0.02$ for wind term and $r = -0.56 \pm 0.03$ for pressure term.

During El Nino phase the increase of thermocline depths in the Eastern and Southern Pacific ocean and decrease in Western Pacific reduce the atmospheric pressure gradient, so the trade winds are weakened and even become westerly there. The change of circulation also affects high atmosphere, producing the increase of the axial AAM, which is observed in Fig. 7. The LOD increases up to approximately 0.1 ms at that time.

When El Nino prevails, the maps of PC 4 for pressure (Fig. 6a) demonstrate the regions of positive influence (pressure increase) over Australia, India, Africa, and Amazonia. The negative input is at western coasts of South and North America. With the development of the opposite event – La Nina (Fig. 6e) the picture changes to opposite values.

During El Nino epoch the wind component (Fig. 6b) has pronounced positive patterns with zones of maxima located in the Eastern Pacific at ±30° latitudes, minima located at equator and ±70°. In the Indian Ocean maxima are over Arabian peninsula, India, Madagascar, and ±20°. Minima are over US and Argentina. With development of La Nina the picture inverts. The animated maps show how ENSO propagates over the Earth's oceans and continents, touching even distant regions, like Europe. They can be used for studying interconnections and possibly revealing the precursors of El Nino/La Nina [41].

In Refs. [21–23,42], the latitude-time Hovmoeller plots were used to demonstrate the polar propagation of ENSO pattern in axial wind AAM term. It had been related to the ocean surface temperature changes and tropospheric wind in response to it. We also found the so-called V-shaped (better to say C-shaped) signatures in latitudinal-averaged Hovmoeller plot for PC 4 of wind (Fig. 8). However, it does not give the complete picture, but only its projection. The animated maps demonstrate that there is no direct polar propagation of AAM along the meridians, but the periodic change in the sign of the anomalies (Fig. 6).

During El Nino epoch the positive and negative wind anomalies, especially well seen in the Pacific Ocean, propagate to the East. But with El Nino phase changing to La Nina, the sign of the anomalies slowly inverses (Fig. 6c,d). The momentum flow from positive to former negative zones (located approximately in tesseral order) makes the effect observed in longitudinal projection as a polar propagation of the atmospheric momentum.

PC 5 of pressure (9 + 10 SN) has a period of 4 months. Its overall minimum is in December, April, and August with the negative input coming from Northern Africa, Europe, Asia, except India, central Amazonia, and Antarctica. Positive input comes from South Africa, Mexico, India, and Australia. The picture inverts with half period of 2 months.

PC 5 of wind (9 + 10 SN) has very complicated patterns, changing with period of 4 months. We will not describe it here.

PC 6 of wind (11 + 12 SN) has period of approximately 2 years and is related to the QBO (quasi-biennial oscillation) teleconnected to ENSO [22,43–45]. The maps of PC 6 demonstrate the patterns, which are very similar to those of PC 4, with polar propagation of momentum from equator to the tropics. We filtered SOI sequentially by the Panteleev filters with parameters $f_0 = 0.3$ and f_0=1 yrs^{-1}, subtracted one signal from another and compared the obtained signal in 0.5 yrs^{-1} frequency band with PC 6. The changes correspond well to each other. Coefficient of correlation was found to be $r = -0.52 \pm 0.02$.

Pressure PC 6 (11 + 12 SN) is also biennial and has similar behavior as PC 4, but with smaller period. Its amplitude is given in Table 1.

Finally, *PC 7*, coming from SN 8, can be attributed to low-frequency ENSO variability. Fingerprints for both wind and

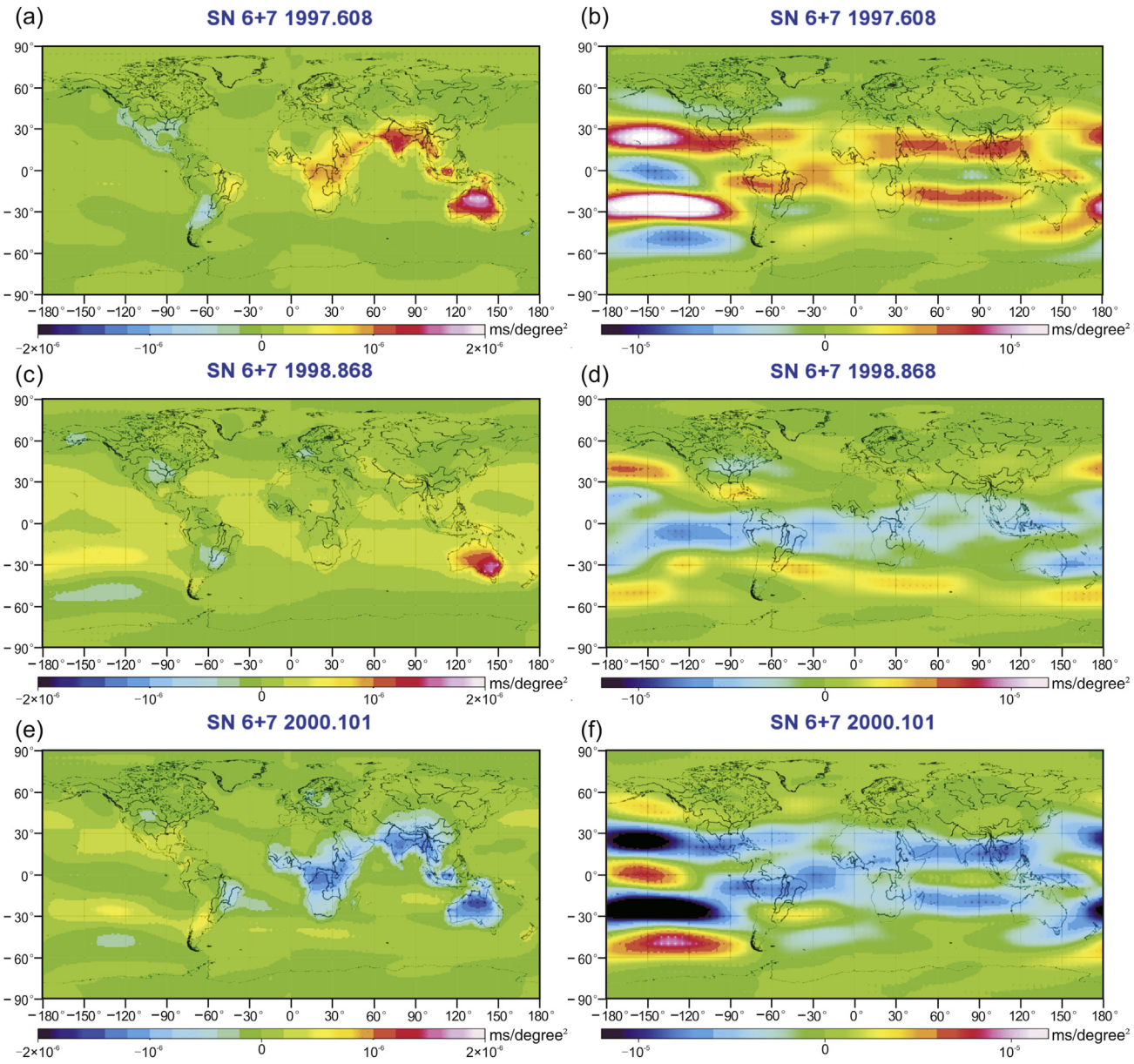

Fig. 6. The three maps of PC 4 for pressure (a,c and e) and wind (b, d and f). The maps on the top correspond to the developed El Nino phase, on the bottom to La Nina. The maps in the middle row show the transition phase, with sign of negative and positive anomalies changing. Depicted evolution creates the effect of polar propagation of momentum for AAM wind component.

pressure are similar to fingerprints of PC 4 and PC 6. There are periods from 3 to 15 years in this PC, but they are not very well separated from biennial variability, as seen in the wind term. The amplitude of this component is rather small (Table 1).

5. Conclusions

In this work, for the first time the joint MSSA of wind and pressure axial AAM maps was performed, allowing us to extract coupled changes in both terms. The PCs with periods 5, 2, 1, 1/2, 1/3 of a year were shown to have been effectively separated from the low-frequency trend and noises. Their animated maps were obtained. Low-frequency, 5- and 2-year PCs reflect the changes of wind and pressures over the globe in the ENSO and QBO cycles covering different frequency bands. Animated maps for these PCs help to track the changes, which cannot be reduced to the simplified explanation of zonal polar propagation of the momentum. This extends the results of Ref. [22,23,42]. The ENSO influence on LOD is found to be at the 0.1 ms level.

The animated maps addressed various meteorological and climatological questions, such as annual air mass redistribution, zonal winds circulation changes, patterns of El Nino at different continents and its precursors. In this article, relying on study of Ref. [2], we have just briefly described the main features of zonal circulation, revealed by the PCs.

The obvious application of the obtained results is to study the changes of Earth's rotation rate. Each pattern on the PCs maps make an input into the integrated EAAM, being directly transferred to LOD changes according to Eq. (1). Initial AAM data could incorporate some observational noises and modelling errors, but MSSA helps to filter them out and produce improved signal decompositions.

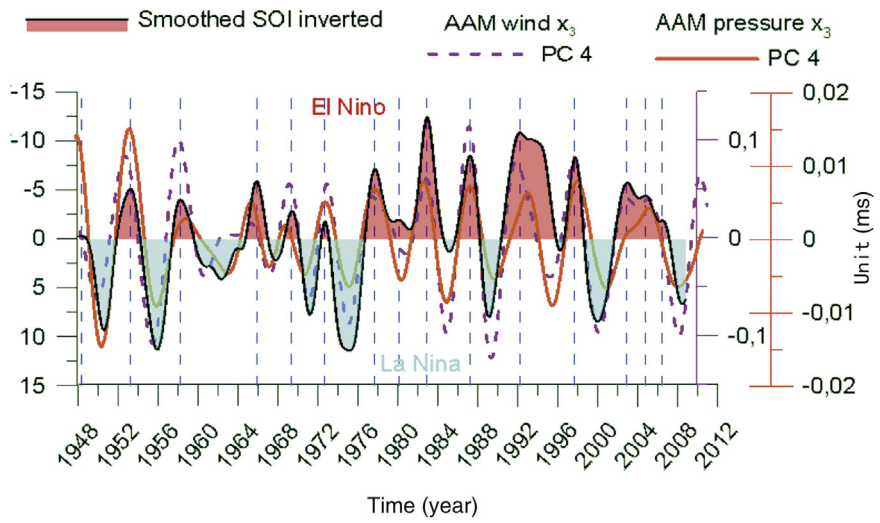

Fig. 7. AAM PC 4 for pressure and wind integrated over the globe, compared to the filtered and inverted SOI index.

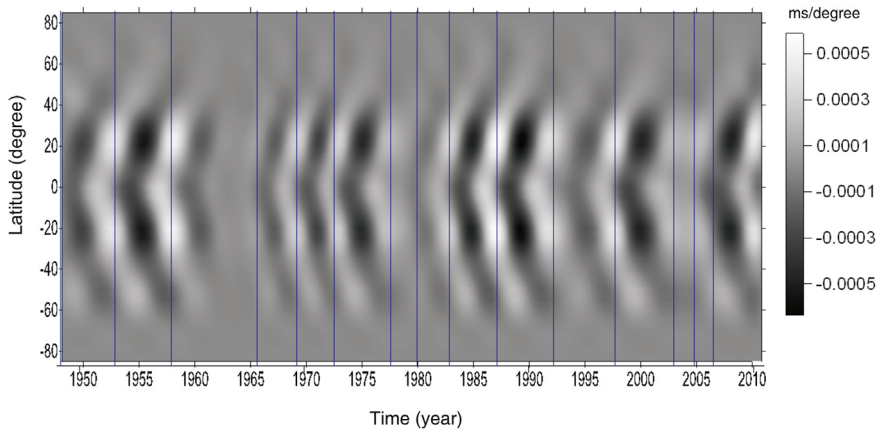

Fig. 8. Latitude-time Hovmoeller plot for the wind PC 4. C-shape of light and dark regions refers to the polar propagation of longitudinal-averaged momentum. The maxima of filtered and inverted SOI, corresponding to El Nino, are marked with vertical grid lines.

We tried to collect empirical arguments to answer the important scientific question: does climate change and its natural variability induce atmospheric circulation changes, influencing the Earth rotation? Our study confirms that the main planetary climate oscillations, such as ENSO, biennial and multidecadal oscillations, are reflected in zonal circulation of the atmosphere, and can be transferred to LOD.

The revealed low-frequency component PC 3 (Fig. 5) is probably related to the trends in wind and pressure fields for the period 1948–2011. AAM pressure increase on the continents and westerly winds strengthen, especially in the southern hemisphere, produced approximately 0.02 acceleration and approximately 0.25 ms deceleration effect, resulting in LOD increase in 60 yrs. This result qualitatively agrees with the results of Ref. [11], which predicts the influence of climate change on LOD variations. Though it is hard to exclude the influence of AAM processing artefacts, noises, etc., we speculate that global warming can modulate the main climatological circulation modes. However, it does not explain anticorrelation between decadal changes in Earth temperature and LOD (Fig. 1a), see Ref. [12]. Further research should clarify this issue.

Besides the axial AAM, the equatorial components influencing the polar motion (PM) are of particular interest. Their analysis is preferred for the annual and Chandler frequency bands [46].

One aim of this article is to demonstrate the strength of MSSA and its usefulness for multidimensional time series processing. Another is in detecting significant signals in AAM. In the next paper we will try to apply these techniques to the longer extent (100 years) ECMWF AAM fields.

Acknowledgements

This work is supported by Russian Foundation for Basic Research grants No. 17-05-00989, No. 16-05-00753, NRU HSE and visiting grants positions at Paris observatory and Wuhan university for the first author. The Ohio State University (OSU) component of the research was partially supported by grants by NSF/IGFA Belmont Forum Project (Grant No. ICER-1342644), and by the Chinese Academy of Sciences/SAFEA International Partnership Program for Creative Research Teams (Grant No. KZZD-EW-TZ-05). We are especially thankful to Y.H. Zhou from Shanghai Observatory for providing AAM data grids. We thank the anonymous reviewers and the editor for their constructive comments which have led to an improved manuscript.

Appendix A. Supplementary data

Supplementary data related to this article can be found at http://dx.doi.org/10.1016/j.geog.2017.02.010.

References

[1] D. Salstein, Atmospheric excitation of polar motion, ASP Conf Ser 208 (2000) 437–446.
[2] N.S. Sidorenkov, The interaction between Earth's rotation and geophysical processes, Wiley-VCH Verlag, Weinheim, 2009.
[3] Zhong Min, Yan Haoming, Zhu Yaozhong, The investigation of atmospheric angular momentum as a contributor to polar wobble and length of day change with AMIP II GCM data, Adv Atmos Sci 19 (2) (2002) 287–296.
[4] G. Petit, B. Luzum, IERS Conventions, 2010. Technical Note No 36.
[5] B.F. Chao, On the excitation of the Earth's polar motion, Geophys Res Lett 12 (8) (1985) 526–529.
[6] A. Brzezinski, Ch. Bizouard, S. Petrov, Influence of the atmosphere on Earth rotation: what new can Be learned from the recent atmospheric angular momentum estimates? Surv Geophys 23 (1) (2002) 33–69.
[7] J. Nastula, D.A. Salstein, Regional geophysical excitation functions of polar motion over land areas, Geodesy Planet Earth Int Assoc Geodesy Symposia 136 (3) (2012) 499–505.
[8] M. Schindelegger, J. Bohm, D. Salstein, H. Schuh, High-resolution atmospheric angular momentum functions related to Earth rotation parameters during CONT08 J, Geod 85 (7) (2011) 425–433.
[9] P. Morgan, R. King, I. Shapiro, Length of day and atmospheric angular momentum: a comparison for 1981–1983, J Geophys Res 90 (B14) (1985) 12645–12652.
[10] T.M. Eubanks, J.A. Steppe, J.O. Dickey, P.S. Callahan, A spectral analysis of the Earth's angular momentum budget, J Geophys Res 90 (B7) (1985).
[11] O. de Viron, V. Dehant, H. Goosse, M. Crucifix, Participating CMIP modeling groups, effect of global warming on the length-of-day, Geophys Res Lett 29 (7) (2002), http://dx.doi.org/10.1029/2001GL013672.
[12] L. Zotov, C. Bizouard, C.K. Shum, A possible interrelation between Earth rotation and climatic variability at decadal time-scale, Geodesy Geodyn 7 (3) (2016) 216–222, http://dx.doi.org/10.1016/j.geog.2016.05.005.
[13] L.V. Zotov, Sea level and global Earth temperature changes have common oscillations, Odessa Astron Publ 26/2 (2013) 289–291.
[14] N.S. Sidorenkov, C. Bizouard, L. Zotov, D. Salstein, Atmospheric angular momentum, Priroda 4 (2014) 22–28.
[15] Cecile Penland, Michael Ghil, Forecasting northern hemisphere 700-mb geopotential height anomalies using empirical normal modes, Mon Wea Rev 121 (1993) 2355–2372.
[16] Geophys. Monogr. Ser., 189, 216D.-Z. Sun, F. Bryan (Eds.), Climate dynamics: Why does climate Vary?, AGU, Washington, D. C., 2010, http://dx.doi.org/10.1029/GM189.
[17] B. Wouters, E. Schrama, Improved accuracy of GRACE gravity solution through empirical orthogonal function filtering of spherical harmonics, Geophys Res Lett 34 (2007) L23711.
[18] E.S. Ince, M.G. Sideris, E. Rangelova, Deriving long-term sea level variations at tide gauge stations in Atlantic North America, Eos Trans AGU 90 (22) (2009). Jt. Assem. Suppl, Abstract CG73A-01.
[19] L. Zotov, Application of Multichannel singular spectrum analysis to geophysical fields and astronomical images, Adv Astronomy Space Phys 2 (1) (2011) 082–084 [Kyiv, Ukraine].
[20] J.O. Dickey, S.L. Marcus, J.A. Steppe, R. Hide, The Earth's angular momentum budget on subseasonal time scales, Science 255 (1992) 321–324.
[21] J.O. Dickey, P. Gegout, S.L. Marcus, Earth-atmosphere angular momentum exchange and ENSO: the rotational signature of the 1997-98 event, Geophys Res Lett 26 (16) (1999) 2477–2480.
[22] J.O. Dickey, S.L. Marcus, O. de Viron, Coherent interannual and decadal variations in the atmosphere-ocean system, Geophys Res Lett 30 (11) (2003) 27–31.
[23] R.X. Black, D.A. Salstein, R.D. Rosen, Interannual modes of variability in atmospheric angular momentum, J Clim 9 (1996) 2834–2849.
[24] W. Munk, G. MacDonald, The rotation of the Earth, Cambridge Univ. Press, 1960.
[25] K. Lambeck, The Earth's variable rotation; geophysical causes and consequences, Cambridge University Press, 1980.
[26] R.S. Gross, Earth rotation variations ?long period, in: T.A. Herring (Ed.), Physical geodesy, Treatise on geophysics, vol. 11, Elsevier, Amsterdam, 2007.
[27] T.M. Eubanks, Variations in the orientation of the Earth, american geophysical union monograph, Geodyn Ser 24 (1993).
[28] Y.H. Zhou, D.A. Salstein, J.L. Chen, Revised atmospheric excitation function series related to Earth's variable rotation under consideration of surface topography, J Geophys Res 111 (2006) D12108, http://dx.doi.org/10.1029/2005JD006608.
[29] R.D. Rosen, D.A. Salstein, Contribution of stratospheric winds to annual and semiannual fluctuations in atmospheric angular momentum and the length of day, J Geophys Res 90 (D5) (1985) 8033–8041.
[30] L. Zotov, Theory of filtering and time series processing, course of lectures, Moscow State University, 2010. http://lnfm1.sai.msu.ru/grav/english/lecture/filtering/.
[31] I.T. Jollife, Principal component analysis, Springer, 2001.
[32] M. Ghil, R.M. Allen, M.D. Dettinger, et al., Advanced spectral methods for climatic time series, Rev Geophys 40 (1) (2002) 1–41.
[33] N. Golyandina, V. Nekrutkin, A. Zhigljavsky, Analysis of Time Series Structure SSA and Related Techniques, CHAPMAN & HALL/CRC, 2001.
[34] E. Rangelova, W. van der Wal, M.G. Sideris, P. Wu, Spatiotemporal analysis of the GRACE-derived mass variations in north America by means of Multichannel Singular spectrum analysis, gravity, geoid and Earth observation, International Association of Geodesy Symposia 135, Springer-Verlag, Berlin, Heidelberg, 2010.
[35] L.V. Zotov, C.K. Shum, N.L. Frolova, in: Sh. Jin (Ed.), Gravity changes over Russian rivers basins from GRACE, in planetary exploration and science: Recent results and advances, Springer, 2014.
[36] S.A. Golyadina, Method “Caterpillar-SSA”: prediction of the time series, Snt-Petersburg, in Russian, 2004.
[37] L. Zotov, C.K. Shum, Singular spectrum analysis of GRACE observations, Eos Trans AGU 90 (22) (2009). Jt. Assem. Suppl, Abstract J11B-02.
[38] E. Boergens, E. Rangelova, M.G. Sideris, J. Kusche, Assessment of the capabilities of the temporal and spatiotemporal ICA method for geophysical signal separation in GRACE data, J Geophys Res Solid Earth 119 (2014) 4429–4447, http://dx.doi.org/10.1002/2013JB010452.
[39] J.P. Peixoto, A.H. Oort, Physics of climate, Rev Mod Phys 56 (3) (1984) 365–429.
[40] K.A. Kulikov, Earth rotation (in Russian), Nedra, Moscow, 1985.
[41] E.N. Voskresenskaya, O.V. Marchukova, Qualitative classification of the La Nina events, Phys Oceanogr 3 (2015) 14–24.
[42] K.C. Mo, J.O. Dickey, S.L. Marcus, Interannual fluctuations in atmospheric angular momentum simulated by the National Centers for Environmental Prediction medium range forecast model, J Geophys Res 102 (1997) 6703–6713.
[43] C. Penland, De. Zh. Sun, A. Capotondi, D.J. Vimont, A brief introduction to El nino and La Nina,Climate dynamics: why does climate Vary?, Geophys. Monogr. Ser., 189, 216, AGU, Washington, D. C, 2010.
[44] Wu Yun-Hao, Spatio-Temporal Variations of Sea-Level for ENSO: Intercomparison Study of Geodetic Satellite Data, Doctoral Dissertation, 2010.
[45] Y. Pan, W.-B. Shen, H. Ding, C. Hwang, J. Li, T. Zhang, The quasi-biennial vertical oscillations at global GPS stations: identification by Ensemble empirical mode decomposition, Sensors (Basel, Switzerland) 15 (10) (2015) 26096–26114, http://dx.doi.org/10.3390/s151026096.
[46] L.V. Zotov, C. Bizouard, On modulations of the Chandler wobble excitation, J Geodyn 62 (2012) 30–34, http://dx.doi.org/10.1016/j.jog.2012.03.010.

Leonid Zotov, Associate professor of National Research University, Highers School of Economics, scientific researcher at Sternberg Astronomical Institute, Lomonosov Moscow State University. Scientific interests: Earth rotation, gravimetry, GRACE, climate change, mathematical filtering.